ELSEVIER

Journal of Magnetism and Magnetic Materials 225 (2001) 337–345

Journal of magnetism and magnetic materials

www.elsevier.com/locate/jmmm

Irreversible magnetization in nickel nanoparticles

P. Zhang[a], F. Zuo[a,*], F.K. Urban III[b], A. Khabari[b], P. Griffiths[b], A. Hosseini-Tehrani[b]

[a] *Department of Physics, University of Miami, Coral Gables, FL 33124, USA*
[b] *Department of Electrical Engineering, Florida International University, Miami, FL 33199, USA*

Received 22 September 2000; received in revised form 20 October 2000

Abstract

We report magnetic studies on nickel nanoparticle films of average particle size of 10 nm. Magnetization as a function of field and temperature show that the system behaves like a random magnet with a strongly field-dependent irreversible temperature, below which the magnetization relax logarithmically with time. The effective barrier extrapolated increases strongly with temperature for a given field. The time dependence suggests the dominant dipole–dipole interaction in this magnetic nanoparticle system. © 2001 Elsevier Science B.V. All rights reserved.

PACS: 75.10.Nr; 75.50.Kj; 75.60.−d; 75.70.Ak

Keywords: Nanoparticles; Magnetization; Irreversible temperature; Dipolar interaction; Magnetic relaxation

1. Introduction

Magnetic nanoparticles are of considerable interest because of both fundamental physics involved and technical applications in diverse areas such as the magnetic storage media, ferrofluids, and catalysts [1–7]. The dynamics of the nanoparticles has been the subject of numerous experimental and theoretical studies. Ferromagnetic particles with diameter in the range of 1–100 nm become monodomain due to the competition between dipole and exchange interactions. Below this critical size, the energy loss due to magnetic domain wall (which is proportional to d^2) is larger than the energy gain due to the dipole magnetic-field energy (proportional to d^3) and surface effect becomes important [8,9]. The monodomain particles behave like a single large magnetic moments with thousands of Bohr magnetons. Because of usually large separation between the particles, the exchange interaction can be neglected. The magnetic properties are determined mostly by dipole field energy and thermal and magnetic anisotropy energies. At finite temperatures, these particles usually exhibit superparamagnetic relaxation dependent on the particle size and temperature. At low temperatures, quantum tunneling of the spin has been reported in several systems [10–13].

A typical feature found in the magnetic nanoparticles is the irreversible magnetic behavior below an irreversibility line or field-dependent blocking temperature [1,2]. The irreversibility line can be found experimentally by measuring the

*Corresponding author. Tel.: +1-305-284-2323; fax: +1-305-284-4222.
E-mail address: fzuo@miami.edu (F. Zuo).

0304-8853/01/$ - see front matter © 2001 Elsevier Science B.V. All rights reserved.
PII: S0304-8853(00)01379-2

magnetization under field cooling or zero field cooling conditions. Above the irreversible temperature, the magnetization is reversible and symmetric. Below the irreversibility line, magnetization depends strongly on the thermal and field history and the hysteresis loop is highly asymmetric about zero field and zero moment. Depending on the nanosystem studied, various time dependence of magnetic relaxations have been reported [1–6,11]. The time dependence can be used to infer the interaction between the nanoparticles.

We have carried out extensive magnetic measurements on several nickel nanoparticle films. The particles have an average size of about 10 nm. Magnetic hysteresis measurements at low temperatures find the coercivity field is about 800 G at 5 K. The magnetization displays strong thermal and field hysteresis with the irreversible temperature decreasing strongly with increasing field. Magnetic relaxation shows a logarithmic time dependence with a strongly temperature-dependent effective barrier. The results are qualitatively consistent with the model of dipole–dipole interaction for the dynamics of this nanoparticle system.

2. Sample preparation and experimental procedure

Fig. 1 shows a schematic diagram of the main features of the differentially pumped deposition system [14]. There are three vacuum chambers which communicate by low conductance connections and which are maintained at three successively lower pressures by differential pumping. From the right to the left in the figure, the pressures are approximately 1, 1×10^{-3} and 1×10^{-4} Torr. The rightmost is the liquid nitrogen cooled wall source chamber into which an adjustable mixture of ultra high purity He and Ar are admitted under computer control. A 3″ diameter magnetron sputtering source is mounted in this chamber to provide a source of sputtered species into the chamber. The temperature of the top and bottom of the external (in-air) flange is monitored using two thermocouples and a computer data acquisition system. Under appropriate conditions, the sputtered species partially condense into nanoparticles in the source chamber and are swept into the middle chamber by the flowing Ar. A low velocity beam of the gas and nanoparticles is thus formed as they escape through the converging-diverging exit nozzle which is 3 mm in diameter at the throat. The middle region is pumped by a cryopump and normally operates at just below 1×10^{-3} Torr depending on gas flow rates. In principle, large heavy species (nanoparticles) will go straight through this region while most of the lighter gas (Ar, He, air) will scatter to random directions and be pumped out. Thus the middle chamber is where

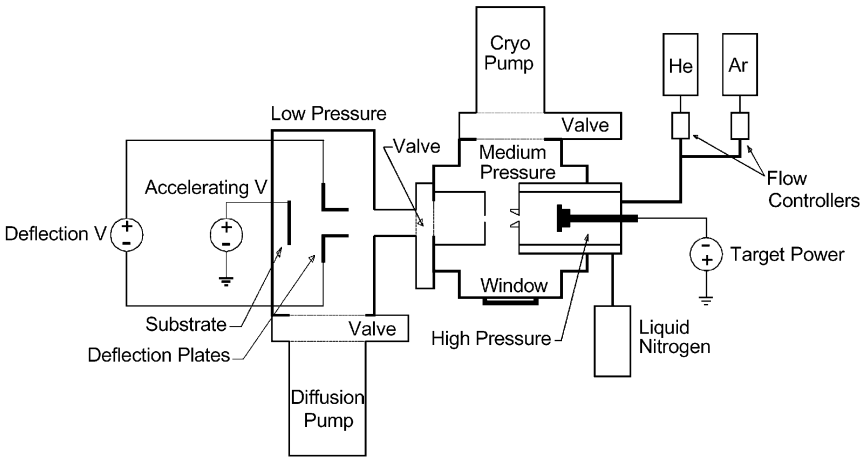

Fig. 1. Schematics of the nanoparticle deposition system.

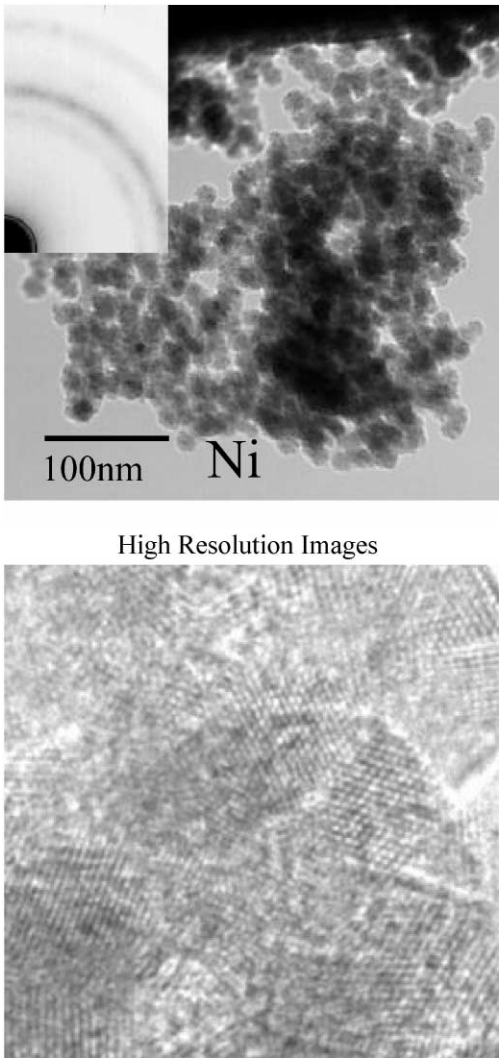

Fig. 2. TEM image of the nickel nanoparticles.

most of the separation of process gas and nanoparticles takes place. The beam of nanoparticles and a small amount of gas enter the diffusion-pumped deposition chamber through an aligned aperture. This region is maintained in the low 10^{-4} Torr range. Beam ionization, deflection, and acceleration electrode assemblies are mounted within the deposition chamber. These apparatus are more fully described elsewhere [15]. The nickel nanoparticles are sputtered to silicon glass substrate. Fig. 2 shows a typical transmission electron microscopy image and high resolution image of the nickel film studied. While the film is spatially inhomogeneous, the average size of these particles is about 10 nm.

The DC magnetization were measured using a SQUID magnetometer (quantum design, MPMS2). Two samples with dimensions of about 2 mm × 4 mm have been measured. The substrate contribution has been measured separately and subtracted in the data presented. Because of the hysteretic effect of the sample studied, both field-cooled (FC) and zero-field cooled (ZFC) measurements have been performed. FC measurements are done when the sample is cooled in field at room temperature and in ZFC measurements, the sample is first cooled to a low temperature in zero field and a field is then applied. Measurements have been carried out with the sample in both parallel and perpendicular to the field directions.

3. Experimental results and analysis

3.1. Hysteretic magnetization

Fig. 3 shows a typical magnetization curve at a high temperature of 200 K with field applied in both perpendicular and parallel to the film

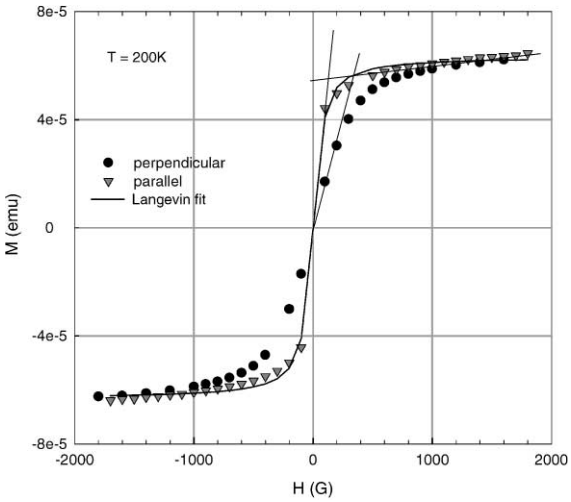

Fig. 3. Magnetization at 200 K for both parallel and perpendicular directions.

directions. For field perpendicular to the film, the saturation field defined by the crossover of the linear extrapolations is about three times larger than in the parallel direction. The large difference can be qualitatively attributed to the larger demagnetization factor in the perpendicular direction. Nevertheless, the crossover field of about 150 G for field parallel to the film direction is much larger than the saturation field ($\sim$2 G) observed for the bulk sample at room temperature. The large saturation field can be attributed to the small size of the nanoparticles. A simple Langevin fit to the data shown by the curve through the data gives an effective number of 1.36×10^5 atoms per particle using the moment of $0.6\,\mu_B$ per atom. Assuming spherical particles, the diameter can be estimated to be about 14 nm, consistent with the TEM results. The thickness of the films varies considerably from the edge to the center, the average thickness from magnetic moment calculation is around 60 nm corresponding to about 4–5 layers of the particles. For perpendicular direction and assuming the ideal demagnetization, the saturation field or demagnetization field is $H = -4\pi M_s \approx 400$ G, considerably smaller than the bulk value of about 6000 G. The difference may be due to combinations of porous nature of the film and oxide layers at the surface.

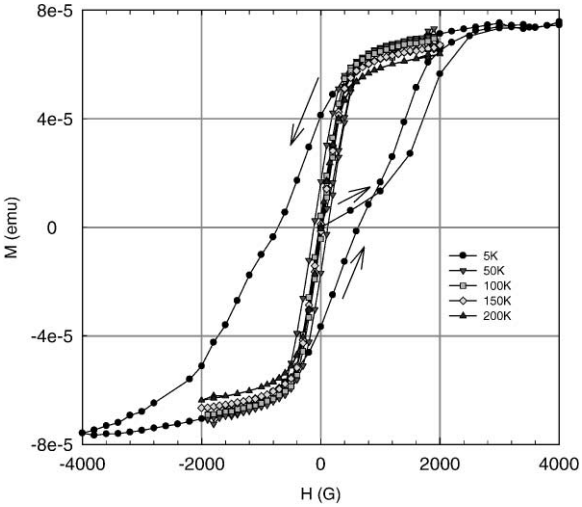

Fig. 4. Magnetic hysteresis at various temperatures for H perpendicular to the film.

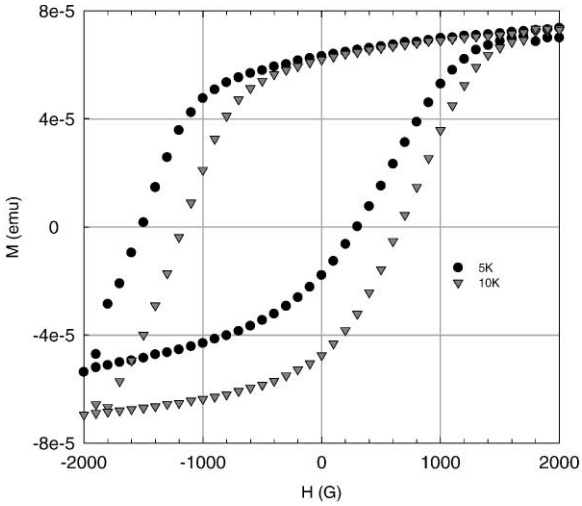

Fig. 5. Asymmetric FC hysteresis at 5 and 10 K.

Fig. 4 shows the temperature dependence of the magnetization from 200 to 5 K in the perpendicular direction. While the hysteresis loops are relatively narrow at 50 and 100 K, the coercivity field increased to about 800 G at 5 K. The hysteresis loop also displays an anomalous field and history dependence in that the virgin magnetization lies outside the hysteresis loop for field above about 900 G. The arrows show the sequences of the magnetization. Similar features have been also observed at higher temperatures where hysteresis are clear.

For FC magnetization, the hysteresis loop is highly asymmetric. Shown in Fig. 5 are the field sweeps at 5 and 10 K. The coercivity field taken as the average of the two directions is nearly the same as in the ZFC case of about 800 G. With an increase in temperature, the asymmetry is reduced as is clear at 10 K.

3.2. Field dependence of irreversible temperature

To further characterize the irreversible magnetization, magnetization as a function of temperature at different fixed fields has been measured. Shown in Fig. 6 is an overlay of magnetization curves at different fields from 50 to 3000 G. For a fixed field, magnetization is measured as a function of temperature for both ZFC and FC. Since the

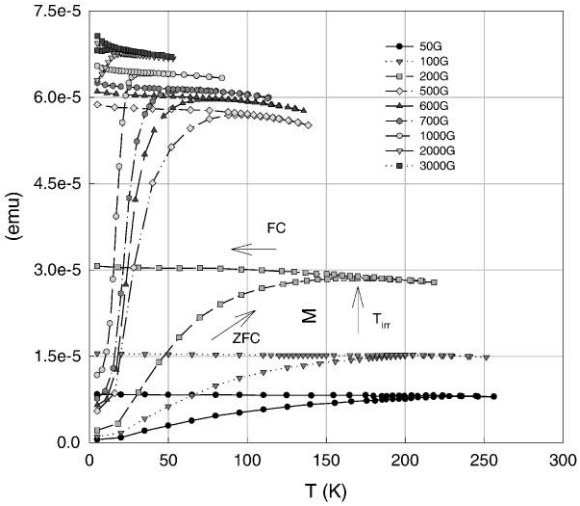

Fig. 6. Irreversible magnetization as a function of temperature at various fields.

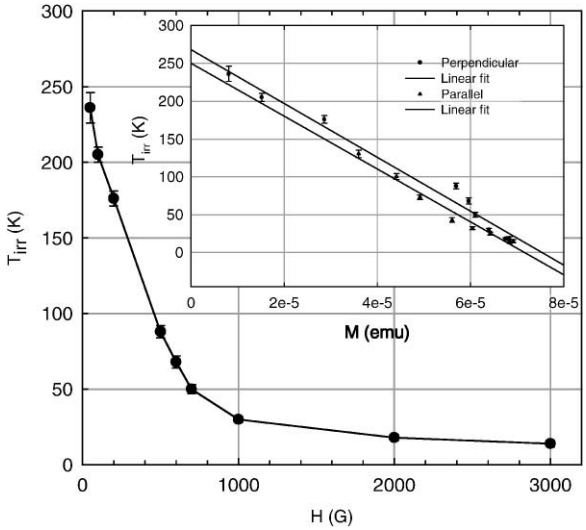

Fig. 7. Irreversibility temperature as a function of field. The inset shows the T_{irr} as a function of magnetic moment for both orientations.

magnetization depends strongly on time, exact definition of the irreversible temperature (often referred as blocking temperature) is not straight forward. Experimentally, we define T_{irr} when the difference between the ZFC and FC magnetizations is less than or equal to 1% of the FC magnetization value, i.e. $M_{FC}(T_{irr}) - M_{ZFC}(T_{irr})/M_{FC}(T_{irr}) \leqq 0.01$. The definition is also close to the instrument resolution of about 10^{-7} emu. For example, at 200 G the ZFC magnetization coincides with the field cooled at an irreversibility temperature T_{irr} of about 175 ± 5 K within the experimental accuracy. ZFC magnetization has a strong temperature dependence below the irreversibility temperature, while the FC magnetization is weakly dependent on temperature. With increasing field, the irreversibility temperature decreases.

Fig. 7 shows the field dependence of the irreversibility temperature as a function of field. For field equal or less than 1000 G, T_{irr} can be fitted with $T_{irr} = T_0 \exp(-H/H_0)$ with $T_0 = 262$ K and $H_0 = 450$ G. If the irreversibility temperature is plotted against the magnetization at T_{irr}, a quasi-linear M dependence is observed for both perpendicular and parallel directions as shown in the inset of Fig. 7. The solid lines are fits to the data with $T_{irr} = T_1(1 - M/M_0)$, with $T_1 = 250$ K, $M_0 = 7.2 \times 10^{-5}$ emu for parallel field direction, and $T_1 = 268$ K, $M_0 = 7.5 \times 10^{-5}$ emu for perpendicular direction.

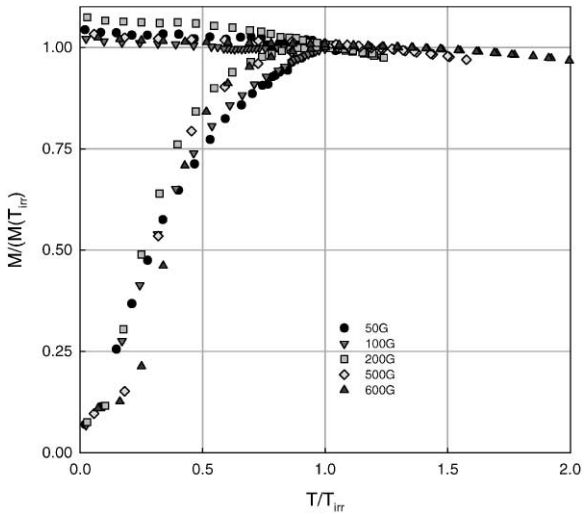

Fig. 8. Normalized magnetization as a function of normalized temperature at various fields.

Fig. 8 plots the scaled magnetization $M/M(T_{irr})$ versus the scaled temperature T/T_{irr}. For $H < 1000$ G, the scaled magnetization curves show a qualitatively good overlap or a scaling behavior, i.e. $M(T,H)/M(T_{irr},H) = f(T/T_{irr})$ with the

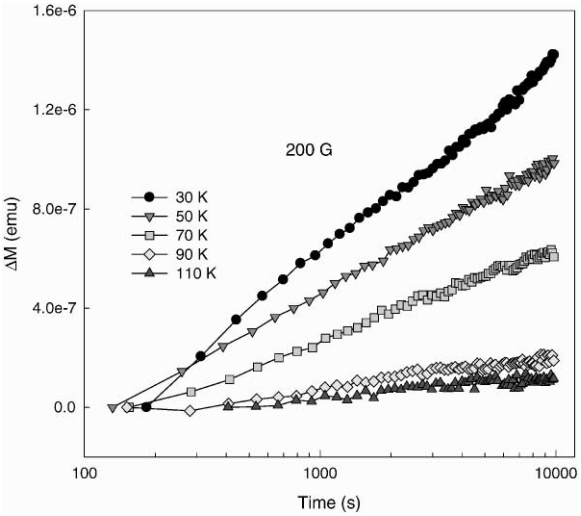

Fig. 9. ZFC magnetic relaxation at various temperatures for $H = 200\,\mathrm{G}$.

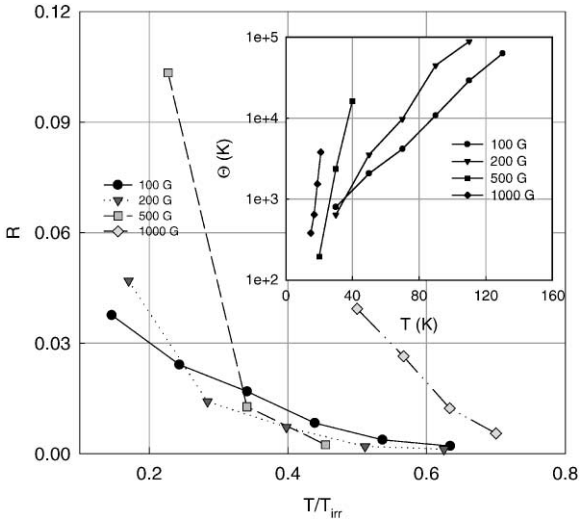

Fig. 10. Normalized magnetic relaxation rate as a function of reduced temperature and field. The inset show the effective barrier as a function of temperature and field.

function f depends only on the reduced temperature.

3.3. Temperature dependence of magnetic relaxation

The irreversibility of the magnetization for the ZFC and FC processes is very similar to the irreversible magnetization in type-II superconductors. To understand the nature of the irreversible magnetization, magnetization as a function of time has been measured extensively for the nanofilm. Shown in Fig. 9 is an overlay of change of magnetization $\Delta M = M(t) - M(t = 0)$ as a function of time in logarithmic scale at temperatures from 30 to 110 K in an applied perpendicular field of 200 G. The time dependence of the magnetization is measured after the sample has been ZFC to a given temperature and the data are collected after a specified field is applied. Clearly, in the time window (nearly 3 h) measured, the magnetization shows $\ln(t)$ dependence. The time dependence of magnetization can be well described by $M(t) = M_0[1 + T/\Theta \ln(t/t_0)]$. The normalized relaxation rate $R = \mathrm{d}M/M_0 d\ln t$ is plotted as a function of reduced temperature T/T_{irr} for different applied field in Fig. 10. In the temperature range measured, the relaxation rate decreases with increasing temperature. The effective barrier Θ as a function of temperature and field is plotted in the inset of Fig. 10 in a semilog scale. For a given field, Θ increases exponentially with temperature.

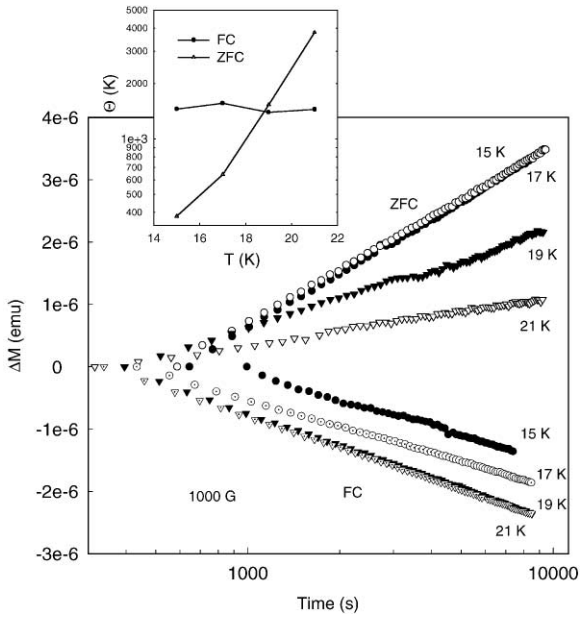

Fig. 11. ZFC and FC relaxation at various temperatures for $H = 1\,\mathrm{kG}$. The inset shows the effective barrier as a function of temperature for both cases.

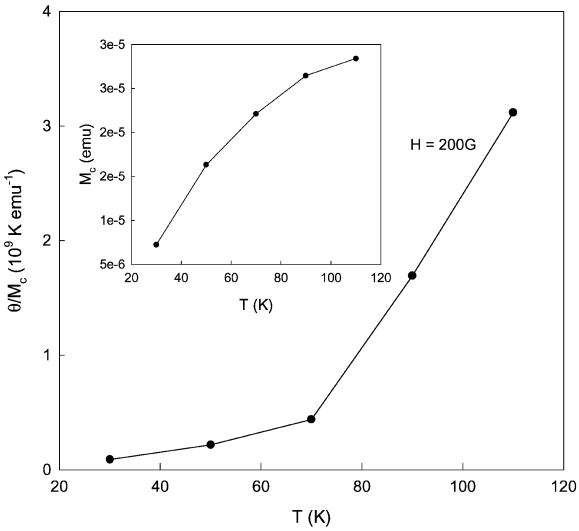

Fig. 12. Scaled effective barrier as a function of temperature. The inset shows the temperature dependence of the M_c at 200 G.

For FC magnetization, similar logarithmic time dependence is observed. Shown in Fig. 11 is an overlay of magnetic relaxation at different temperatures at 1000 G for both ZFC and FC processes. For the ZFC, the relaxation decreases rapidly with increasing temperature while for the FC, the relaxation rate is essentially constant in the similar temperature range.

Shown in the inset of Fig. 12 is the fitted Θ as a function of temperature for the two processes. The barrier height increases exponentially in the ZFC case while nearly constant for the FC case.

4. Discussion

Magnetic irreversibility and logarithmic time dependence has been reported in several magnetic nanoparticle system including γ-Fe_2O_3 nanoparticles of various morphologies [1]. The phenomena is very similar to the magnetic irreversibility in the mixed state of superconductors. The origin of the irreversibility lies in the interplay between the thermal energy and energy barriers separating the different states. In the magnetic nanoparticle system, several models have been discussed to count for the interaction between the particles [16–19].

For noninteracting particles, the magnetic relaxation usually is given by the Néel–Brown expression [20,21] $\tau = \tau_0 \exp(\Delta E/kT)$ where τ_0 is of order of 10^{-9}–10^{-13} s and depends weakly on temperature, ΔE is the energy barrier separating the two easy directions of magnetization, k is the Boltzmann constant and T is the temperature. For particles with uniaxial symmetry the magnetic energy is anisotropic and can be written by $E(\theta) = kV \sin^2(\theta)$ where K is the magnetic anisotropy constant, V is the volume of the particle and θ is the angle between the magnetization and the easy axis. In this case, the energy barrier is given by $\Delta E = KV$.

When the dipole field energy due to the applied field and the neighboring magnetic moments is not negligible compared with the anisotropy energy, the total energy is $E(\theta) = KV \sin^2(\theta) - VM_p H_p \cos(\psi)$, where M_p is the particle magnetic moment per unit volume and H_p is the field at the particle site, ψ is the angle between the magnetic moment and the field and V is the volume of the particle [16–19]. The magnetic field energy reduce the effective barrier to $\Delta E = KV(1 - (M_p H_p/2K)^2$ assuming $\psi = \theta$, thus a faster relaxation toward the equilibrium state. The model assumes a constant H_p for all particles involved which is hardly realized in real systems. To consider the internal field due to the neighboring moment in a quasirandom system is not a trivial problem. It has been suggested that the internal dipole field can be considered proportional to the average magnetic moment, $H_p = H + \gamma M$, here H is the applied field and M is the average moment and γ is the proportional constant. The energy barrier thus can be expressed by

$$\begin{aligned}\Delta E &= KV\left(1 - \frac{M_p(H+\gamma M)}{2K}\right)^2 \\ &\approx KV\left(1 - \frac{M_p(H+\gamma M)}{K}\right) \\ &= U_0(1 - M/M_0)\end{aligned}$$

with

$$U_0 = V(K - M_p H)$$

and

$$M_0 = \frac{K - M_p H}{\gamma M_p}.$$

In this approximation, the time dependence of the magnetization can be expressed as

$$\frac{\partial M}{\partial t} = \frac{M_c}{\tau_0} \exp\left(-\frac{\Delta E}{kT}\right) = \frac{M_c}{\tau_0} \exp\left(-\frac{U_0(1 - M/M_0)}{kT}\right).$$

The equation leads to a logarithmic time dependence of the magnetization given by

$$M(t) = M_c\left[1 + \frac{T}{\Theta}\ln\left(1 + \frac{t}{t_0}\right)\right]$$

where $\Theta = M_c U_0/M_0$ and $t_0 = \tau_0 T/\Theta \exp((U_0 - \Theta/kT))$. The normalized relaxation rate $R = \partial M/M_c \partial \ln t = T/\Theta\ t/(t_0 + t)$.

From the normalized relaxation rate the effective energy barrier Θ can be extracted as shown in Fig. 10. For a given field, the effective barrier increases nearly exponentially with temperature. While part of the temperature dependence is attributed to the temperature dependence of M_c as in $U_0 = M_0\Theta/M_c$, a plot of Θ/M_c, as a function of temperature in Fig. 12 still yields an increasing temperature dependence. The origin of the temperature dependence is not clear since one would expect to the first order a constant U_0 and M_0 from the model above. The temperature dependence may be indicative of a temperature-dependent anisotropy constant K and the assumption of the internal dipole field in the form of γM.

For FC magnetic relaxation, the effective barrier is relatively constant in the temperature range investigated. This is understood by considering the fact that the relaxations take place after the field has been reduced to zero. Since the magnetic moment is weakly dependent on temperature in FC processes, the constant effective barrier is thus expected from the model discussed above.

The irreversibility temperature is usually associated with the barrier height dependent on the measurement time and accuracy. If ΔM is the smallest magnetic moment measurable and Δt is the time window for the measurement, the irreversibility temperature can be found

$$T_{irr} = \Theta\frac{1 - \Delta M/M_c}{\ln(1 + \Delta t/t_0)} \approx \frac{\Theta}{\ln(1 + \Delta t/t_0)}.$$

With increasing field, T_{irr} decreases nearly exponentially at small H as in Fig. 7 and linearly with M_{irr} as in the inset of Fig. 7. The linear M_{irr} dependence can in principle be inferred from the field and temperature dependence of Θ, which is related to M_c. Since the irreversible magnetization is shown to scale with the reduced temperature by $M(T,H)/M(T_{irr},H) = f\,(T/T_{irr})$. The ZFC magnetization $M(T,H)$ is in practice very close to the $M_c(T,H)$, thus a linear M_{irr} dependence is expected. Alternatively, a simple thermodynamic argument suggests $kT_{irr} \sim \Delta E = U_0(1 - M/M_0)$ and hence a decreasing irreversible temperature with the increasing magnetization.

The anomalous magnetization hysteresis loop agrees with the picture of randomly pinned magnet moments. The small saturation moment compared to the bulk value suggests that there is a substantial reduction of the magnetic moment due to the presence of surface layers which are either spin disordered or magnetically dead. Further surface characterizations are necessary to pin down the cause. The effect of particle size distribution is another concern in the description of the magnetic relaxation. It has been suggested [10] the distribution of particle size leads to a size-dependent barrier height and thus a logarithmic time dependence. While it is not clear if this model will produce the linear M and H dependence of the irreversibility temperature and barrier height as experimentally obtained, the possibility should not be excluded without further characterization of the films.

In summary, we have reported a careful magnetization measurement on the nickel nanoparticle system. Our results show that the nanosystem behaves like a random magnet with a large field-dependent irreversibility temperature. The nanoparticle behaves like a superparamagnet and a spin glass above and below T_{irr}, respectively. Magnetic relaxation studies show a clear logarithmic time dependence and a strongly field and temperature-dependent effective barrier. The data is qualitatively consistent with the model in which

the time-dependent dipole field dominates the magnetic relaxation in this nanosystem. Further consideration by including the effect of particle size distribution may be necessary to count quantitatively the field and temperature dependence of the irreversible magnetization and spin dynamics.

Acknowledgements

The authors acknowledge very helpful discussions with Drs. G. Alexandrakis, C. Vittoria and S. Barnes. The work is supported in part by NSF grant No. DMR-9623306 and work at Florida International University is supported by NSF DMR-9614882.

References

[1] R. Prozorov, Y. Yeshurun, T. Prozorov, A. Gedanken, Phys. Rev. B 59 (1999) 6956.
[2] J.L. Dormann, D. Fiorani, E. Tronc, Adv. Chem. Phys. 98 (1997) 283.
[3] J.G.S. Lok, A.K. Geim, J.C. Maan, S.V. Dubonos, L. Theil Kuhn, P.E. Lindelof, Phys. Rev. B 58 (1998) 12201.
[4] T. Jonsson, J. Mattsson, C. Djurberg, F.A. Khan, P. Nordblad, P. Svelindh, Phys. Rev. Lett. 75 (1995) 4138.
[5] H. Mamiya, I. Nakatani, T. Furubayashi, Phys. Rev. Lett. 80 (1998) 177.
[6] J. Zhang, C. Boyd, W. Luo, Phys. Rev. Lett. 77 (1996) 390.
[7] A.E. Berkowitz, R.H. Kodama, S.A. Makhlouf, F.T. Parker, F.E. Spada, E.J. MvNiff Jr., S. Foner, J. Magn. Magn. Mater. 196–197 (1999) 591.
[8] B. Martinez, X. Obradors, Ll. Balcells, A. Rouanet, C. Monty, Phys. Rev. Lett. 80 (1998) 181.
[9] D. Schmeiber, O. Bohme, A. Yfantis, T. Heller, D. Batchelor, I. Lundstrom, A.L. Spetz, Phys. Rev. Lett. 83 (1999) 380.
[10] J. Tejada, X.X. Zhang, E.M. Chudnovsky, Phys. Rev. B 47 (1993) 14977.
[11] X.X. Zhang, J.M. Hernandez, J. Tejada, R.F. Ziolo, Phys. Rev. B 54 (1996) 4101.
[12] W. Wernsdorfer, E. Bonet Orozco, K. Hasselbach, A. Benoit, D. Mailly, O. Kubo, H. Nakano, B. Barbara, Phys. Rev. Lett. 79 (1997) 4014.
[13] S. Gueron, M.M. Deshmukh, E.B. Myers, D.C. Ralph, Phys. Rev. Lett. 83 (1999) 4148.
[14] F.K. Urban III, A. Khabari, G. Fernandez, J. Vac. Sci. Tech. A 17 (4) (1999) 2374.
[15] F.K. Urban III, J. Appl. Phys. 67 (11) (1990) 7082.
[16] S. Morup, E. Tronc, Phys. Rev. Lett. 72 (1994) 3278.
[17] M.F. Hansen, S. Morup, J. Magn. Magn. Mater. 184 (1998) 262.
[18] T. Jonsson, P. Nordblad, P. Svelindh, Phys. Rev. B 57 (1998) 497.
[19] M.F. Hansen, F. Bodker, S. Morup, K. Lefmann, K.N. Clausen, P. Lindgård, Phys. Rev. Lett. 79 (1997) 4910.
[20] L. Neel, Ann. Geophys. 5 (1949) 99.
[21] W.F. Brown, Phys. Rev. 130 (1963) 1677.